Supplementary Material (ESI) for *CrystEngComm*
This journal is © The Royal Society of Chemistry

Rational design of four multifunctional octamolybdate-based complexes for detecting different ions and removing organic dyes from aqueous solution

Xiu-Li Wang*, Zi-Wei Cui, Hong-Yan Lin, Zhi-Han Chang

X-ray Crystallographic Study

Single crystal X-ray diffraction analysis data for **1-4** were carried out using a Bruker SMART APEX II CCD diffractometer equipped with Mo-Kα monochromatic radiation (λ = 0.71073 Å) by ω and θ scan mode. All the structures were solved by direct methods with the Olex2 software. [1] The final refinement was performed by full matrix least-squares techniques on F^2. All non-hydrogen atoms were refined with anisotropic temperature parameters. All Hydrogen atoms were placed in geometrically idealized position as a riding mode. Data collection, cell refinement and data reduction for complexes **1-4** were performed in Table 1. For **2** and **4**, to keep the charge in balance, two hydrogen cations are added into the molecular formula. Selected bond distances and angles were summarized in Table S1. The selected hydrogen-bonding distances (Å) and angles (°) for **2** and **4** are presented in Table S2. The CCDC numbers are 1998302, 2047059-2047061.

Preparation of complexes 1-4 bulk-modified carbon paste electrode (1-, 2-, 3-, 4-CPEs)

Complexes **1-4** modified carbon paste electrodes **(1-, 2-, 3-, 4**-CPEs**)** was prepared as follows: graphite powder (0.10 g) and complexes **1-4** (0.01 g) were mixed and ground together in an agate mortar for approximately 45 minutes to get a homogeneous mixture, and then 0.05 mL paraffin oil was added and the mixture was stirred with a glass rod. The uniform mixture was packed into a 3 mm inner diameter glass tube and the tube surface was wiped with weighing paper. The electrical contact was established with copper wire through the back of the electrode.

Table S1. Selected bond distances (Å) and angles (°) for complexes **1-4**.

Complex **1**			
Cu(1)-O(2)	1.922(3)	Cu(2)-O(1)	2.153(4)
Cu(1)-O(2)#2	1.922(3)	Cu(2)-O(1)#3	2.153(4)
Cu(1)-N(1)	1.996(4)	Cu(2)-N(4)#4	2.158(4)
Cu(1)-N(1)#2	1.996(4)	Cu(2)-N(4)#5	2.158(4)
Cu(1)-O(4)	2.534(4)	Cu(2)-N(2)	2.086(5)

Cu(1)-O(4)#2	2.534(4)	Cu(2)-N(2)#3	2.086(5)
O(2)#2-Cu(1)-O(2)	180	N(4)#5-Cu(2)-N(4)#4	93.8(2)
O(2)#2-Cu(1)-N(1)	97.35(16)	N(2)-Cu(2)-O(1)#3	95.05(18)
O(2)-Cu(1)-N(1)	82.65(16)	N(2)#3-Cu(2)-O(1)	95.04(18)
O(2)#2-Cu(1)-N(1)#2	82.65(16)	N(2)-Cu(2)-O(1)	77.40(18)
O(2)-Cu(1)-N(1)#2	97.35(16)	N(2)#3-Cu(2)-O(1)#3	77.41(18)
N(1)#2-Cu(1)-N(1)	180	N(2)-Cu(2)-N(4)#5	168.10(19)
O(1)#3-Cu(2)-O(1)	169.5(2)	N(2)#3-Cu(2)-N(4)#5	89.47(16)
O(1)-Cu(2)-N(4)#4	96.36(16)	N(2)#3-Cu(2)-N(4)#4	168.08(19)
O(1)-Cu(2)-N(4)#5	90.83(16)	N(2)-Cu(2)-N(4)#4	89.47(16)
O(1)#3-Cu(2)-N(4)#4	90.83(16)	O(1)#3-Cu(2)-N(4)#5	96.36(16)
Symmetry codes: #2 -x+1, -y+1, -z+1; #3 -x, y, -z+1/2; #4 -x+1/2, y+1/2, -z+1/2; #5 x-1/2, y+1/2, z			

Complex **2**

Cu(1)-O(1)#2	1.938(6)	Cu(1)-N(1)	1.993(7)
Cu(1)-O(1)	1.938(6)	Cu(1)-O(1W)	2.431(6)
Cu(1)-N(1)#2	1.993(7)	Cu(1)-O(1W)#2	2.431(6)
O(1)#2-Cu(1)-O(1)	180	O(1)#2-Cu(1)-O(1W)#2	94.0(3)
O(1)#2-Cu(1)-N(1)#2	83.2(3)	O(1)-Cu(1)-O(1W)	94.0(3)
O(1)#2-Cu(1)-N(1)	96.8(3)	N(1)-Cu(1)-N(1)#2	180.0(4)
O(1)-Cu(1)-N(1)	83.2(3)	N(1)-Cu(1)-O(1W)#2	83.1(3)
O(1)-Cu(1)-N(1)#2	96.8(3)	N(1)#2-Cu(1)-O(1W)	83.1(3)
O(1)-Cu(1)-O(1W)#2	86.0(3)	N(1)-Cu(1)-O(1W)	96.9(3)
O(1W)-Cu(1)-O(1W)#2	180		
Symmetry codes: #2 -x+2, -y+2, -z+2			

Complex **3**

Cu(1)-O(1)	1.970(3)	Cu(2)-O(3W)	1.980(3)
Cu(1)-O(1W)	1.977(3)	Cu(2)-O(2)	1.983(3)
Cu(1)-O(2W)	1.965(3)	Cu(2)-O(4W)	1.953(3)
Cu(1)-N(1)	1.998(3)	Cu(2)-N(2)	2.010(4)
Cu(1)-N(4)#1	2.444(4)	Cu(2)-N(6)#2	2.372(4)
Cu(1)-O(26)	2.659(3)	Cu(2)-O(24)	2.592(3)
O(1)-Cu(1)-O(1W)	165.56(13)	O(2W)-Cu(1)-N(4)#1	91.04(12)
O(1)-Cu(1)-N(1)	81.78(14)	N(1)-Cu(1)-N(4)#1	97.09(13)
O(1)-Cu(1)-N(4)#1	102.05(13)	O(3W)-Cu(2)-O(2)	172.02(13)
O(1W)-Cu(1)-N(1)	92.01(14)	O(3W)-Cu(2)-N(2)	93.50(14)
O(1W)-Cu(1)-N(4)#1	91.61(13)	O(3W)-Cu(2)-N(6)#2	83.40(13)
O(2W)-Cu(1)-O(1)	91.81(13)	O(2)-Cu(2)-N(2)	81.59(13)
O(2W)-Cu(1)-O(1W)	92.60(13)	O(2)-Cu(2)-N(6)#2	103.52(13)
O(2W)-Cu(1)-N(1)	170.53(14)	O(4W)-Cu(2)-O(3W)	93.02(14)
O(4W)-Cu(2)-N(6)#2	98.04(13)	O(4W)-Cu(2)-O(2)	89.96(13)
N(2)-Cu(2)-N(6)#2	99.08(14)	O(4W)-Cu(2)-N(2)	162.27(14)
Symmetry codes: #1 -x, y-1/2, -z+1/2; #2 -x+1, y+1/2, -z+1/2			

Complex **4**			
Cu(1)-O(1)	1.969(3)	Cu(1)-N(1)#2	1.981(3)
Cu(1)-O(1)#2	1.969(3)	Cu(1)-O(1W)	2.374(4)
Cu(1)-N(1)	1.980(3)	Cu(1)-O(1W)#2	2.374(4)
O(1)#2-Cu(1)-O(1)	180	O(1)-Cu(1)-O(1W)#2	92.00(16)
O(1)#2-Cu(1)-N(1)	97.48(13)	O(1)#2-Cu(1)-O(1W)	92.00(16)
O(1)-Cu(1)-N(1)	82.52(13)	N(1)-Cu(1)-N(1)#2	180.0(2)
O(1)-Cu(1)-N(1)#2	97.48(13)	N(1)#2-Cu(1)-O(1W)	85.44(13)
O(1)#2-Cu(1)-N(1)#2	82.52(13)	N(1)-Cu(1)-O(1W)	94.56(13)
O(1)#2-Cu(1)-O(1W)#2	88.00(16)	N(1)-Cu(1)-O(1W)#2	85.44(13)
O(1)-Cu(1)-O(1W)	88.00(16)	N(1)#2-Cu(1)-O(1W)#2	94.56(13)
O(1W)#2-Cu(1)-O(1W)	180		

Symmetry codes: #2 -x+2, -y+2, -z+2

Table S2 Selected hydrogen bond distances (Å) and angles (°) for **2** and **4**.

	D–H···A	D–H	H···A	D···A	D–H···A
Complex **2**	N(4)–H(4)···O(8)	0.86	2.19	2.927	143
Complex **4**	N(3)–H(3)···O(11)	0.86	2.23	2.957	141

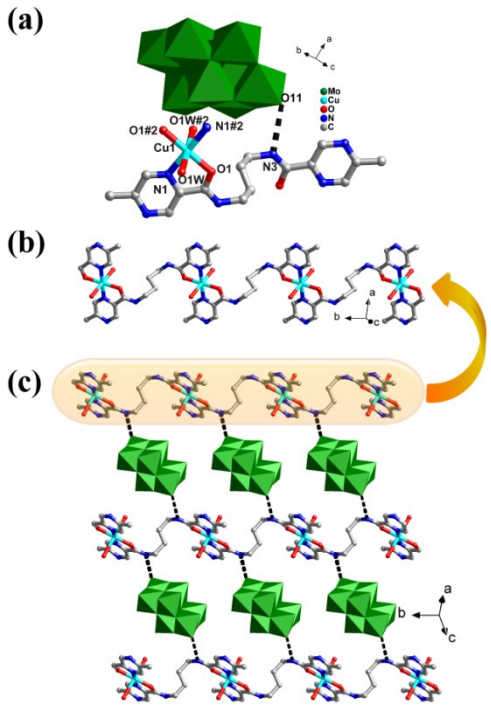

Fig. S1. (a) The coordination environment of Cu^{II} ion in complex **4**. (b) The 1D $[Cu(bmpab)]_n^{2n+}$ of complex **4**. (c) The 2D supramolecular layer of complex **4**

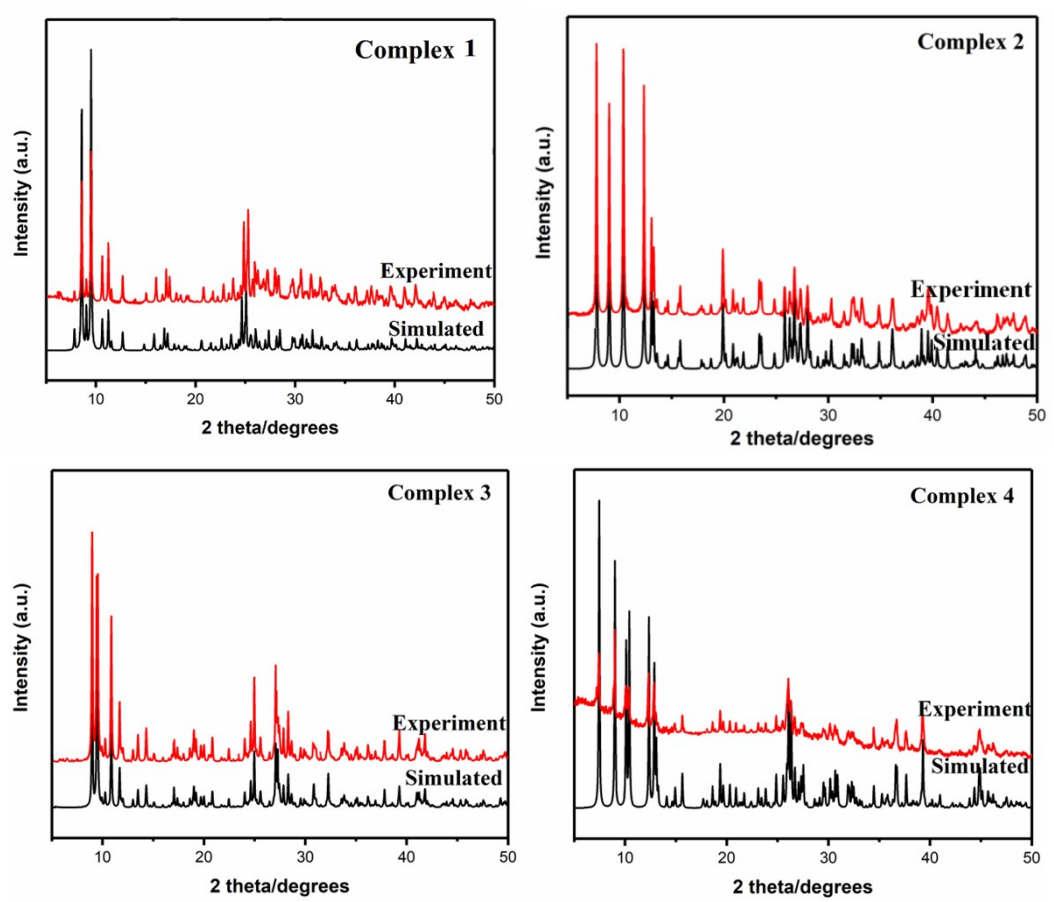

Fig. S2 The PXRD patterns of complexes **1-4.**

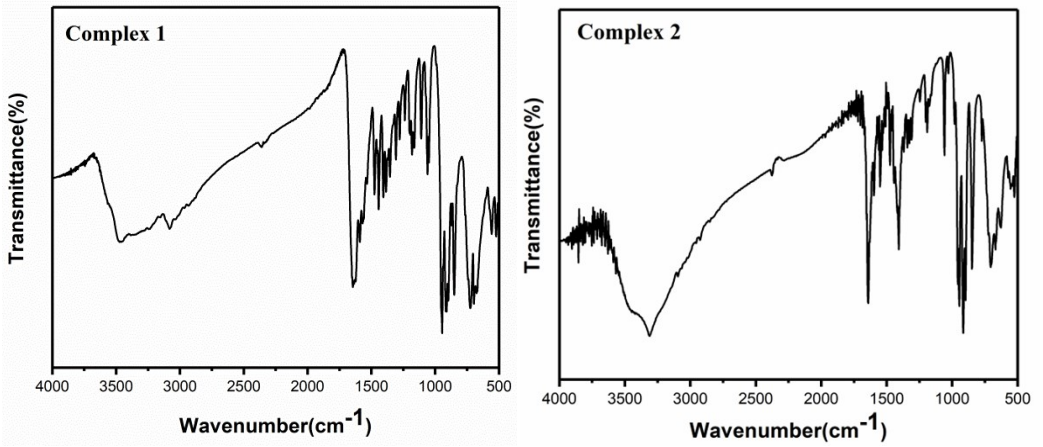

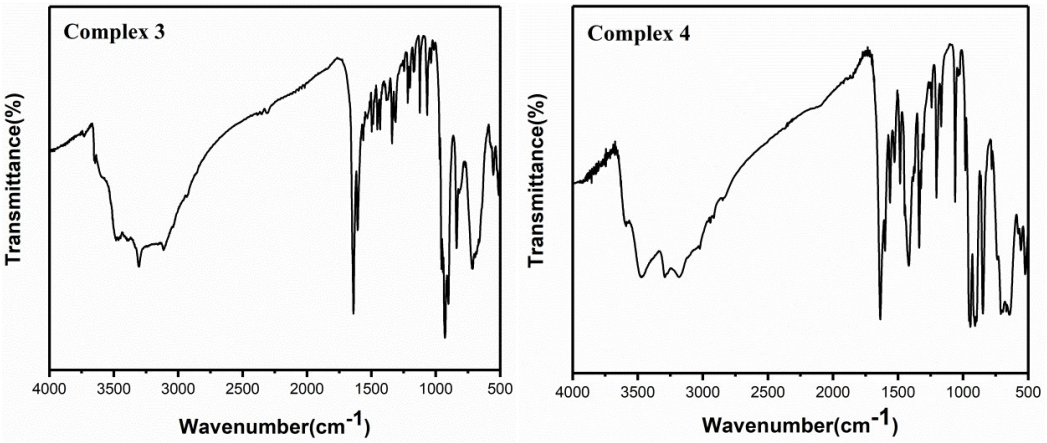

Fig. S3 The IR spectra of complexes **1-4**.

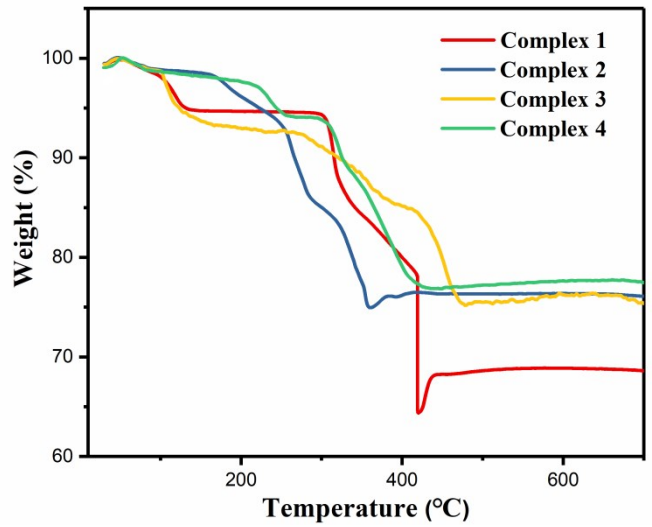

Fig. S4 The TG curves of complexes **1-4**.

Table S3 The average peak potentials of the redox peaks.

	I-I’	II-II’	III-III’
1-CPE	+201	+65	-155
2-CPE	+154	+19	-190
3-CPE	+213	+74	-148
4-CPE	+219	+39	-183
$E_{1/2}= (E_{pa}+ E_{pc})/2$ (scan rate: 60 $mV \cdot s^{-1}$)			

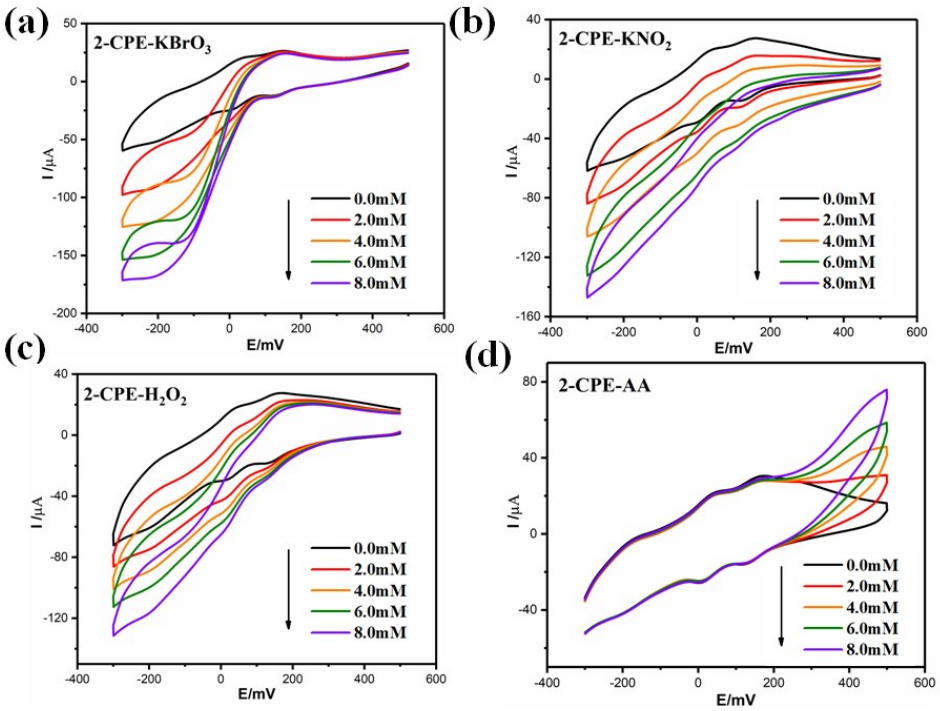

Fig. S5 The cyclic voltammograms of **2**-CPE in 0.1 M H_2SO_4 + 0.5 M Na_2SO_4 electrolyte solution containing $KBrO_3$ (a), KNO_2 (b), H_2O_2 (c) and AA (d) (scan rate: 60 mV s^{-1}).

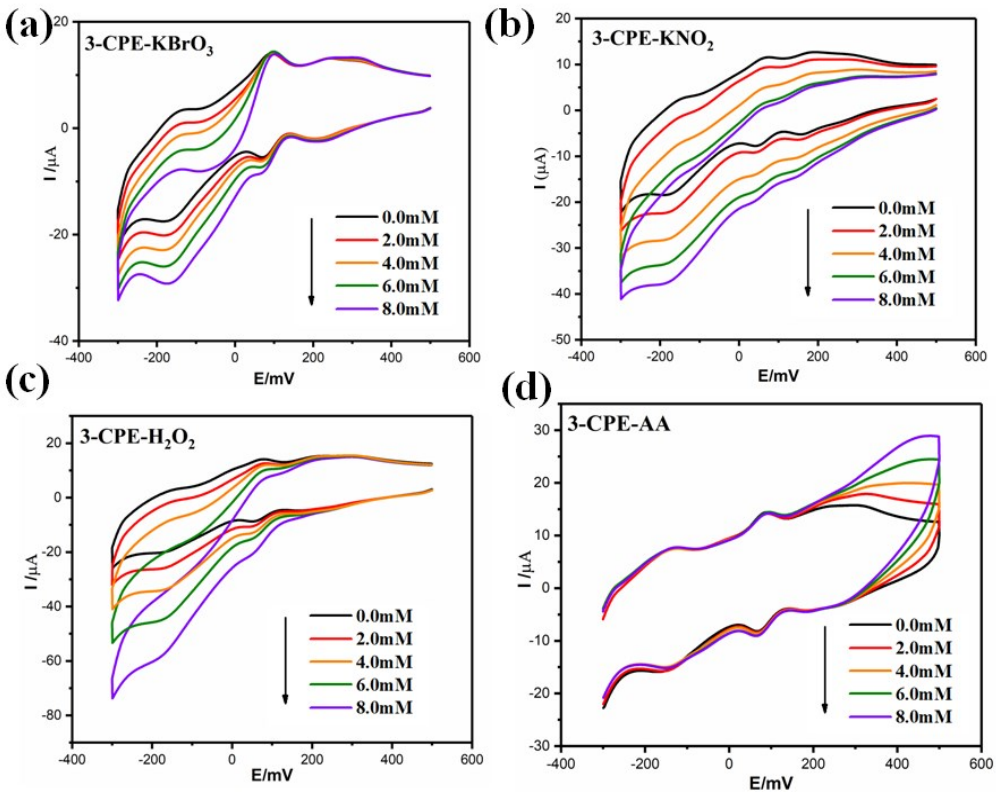

Fig. S6 The cyclic voltammograms of **3**-CPE in 0.1 M H_2SO_4 + 0.5 M Na_2SO_4 electrolyte solution containing $KBrO_3$ (a), KNO_2 (b), H_2O_2 (c) and AA (d) (scan rate: 60 mV s^{-1}).

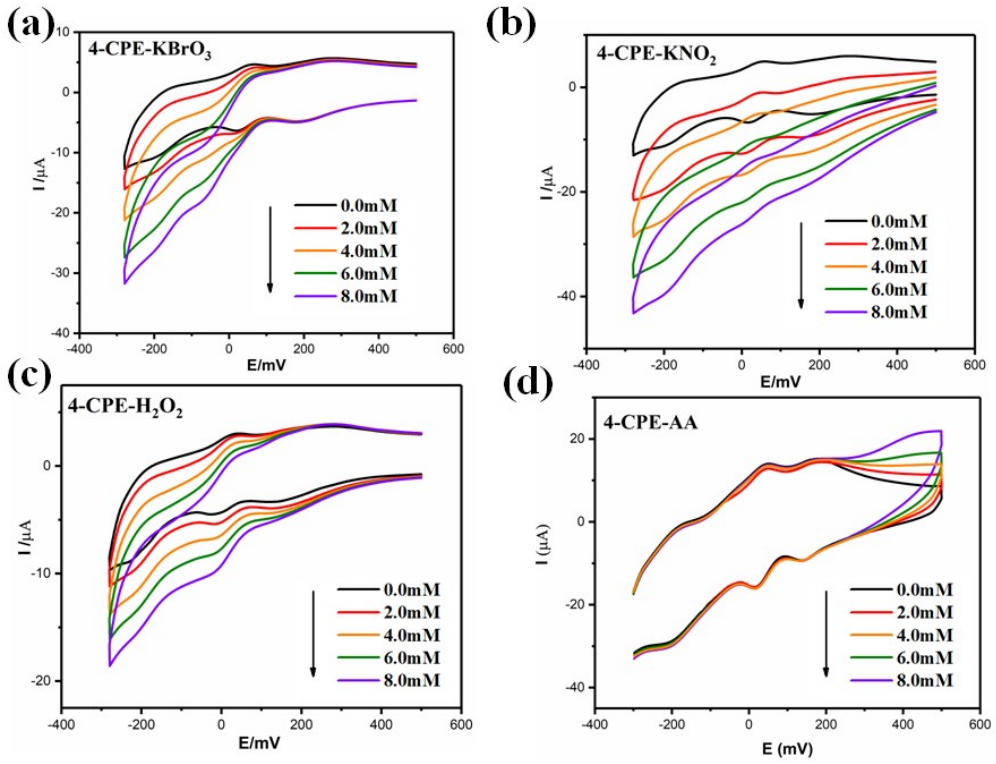

Fig. S7 The cyclic voltammograms of **4**-CPE in 0.1 M H_2SO_4 + 0.5 M Na_2SO_4 electrolyte solution containing $KBrO_3$ (a), KNO_2 (b), H_2O_2 (c) and AA (d) (scan rate: 60 mV s^{-1}).

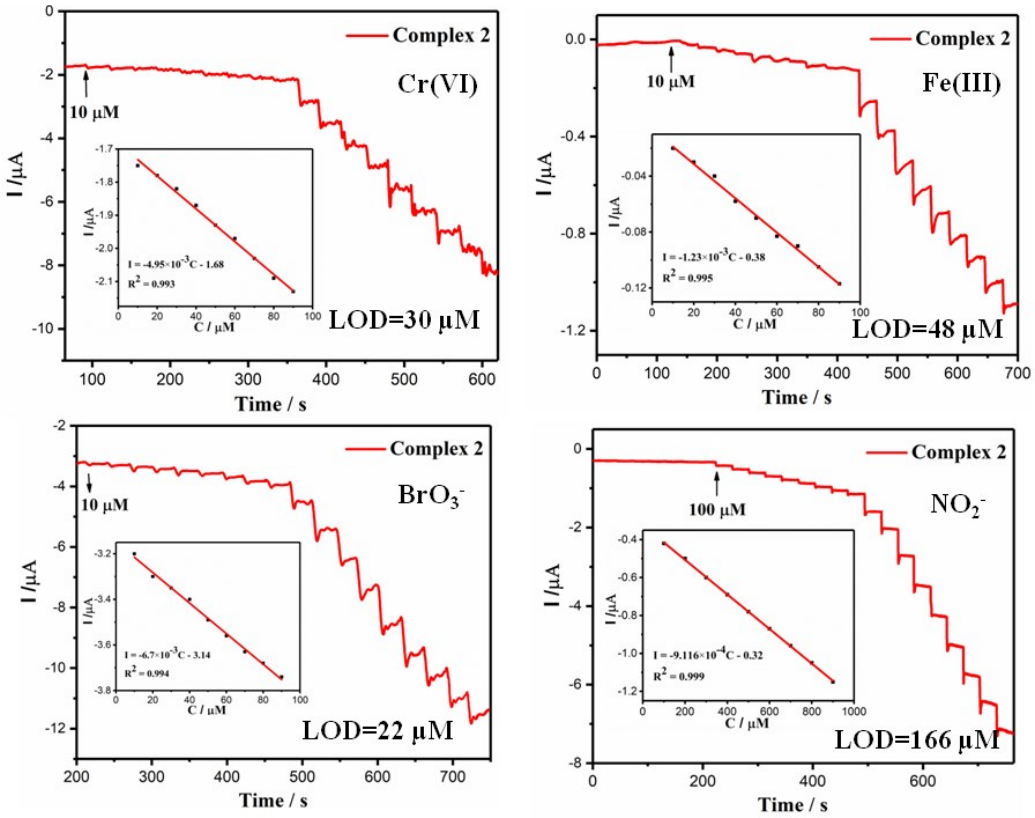

Fig. S8 Current response of **2**-CPE with successive addition of Cr(VI) (a) Fe(III) (b) BrO_3^- (c) and NO_2^- (d) into stirring 0.1 M H_2SO_4 + 0.5 M Na_2SO_4 electrolyte solution per 30 s interval (Inset: the plot of response current *vs.* concentrations of substrate, Applied potential: -200 mV for **2**–CPE).

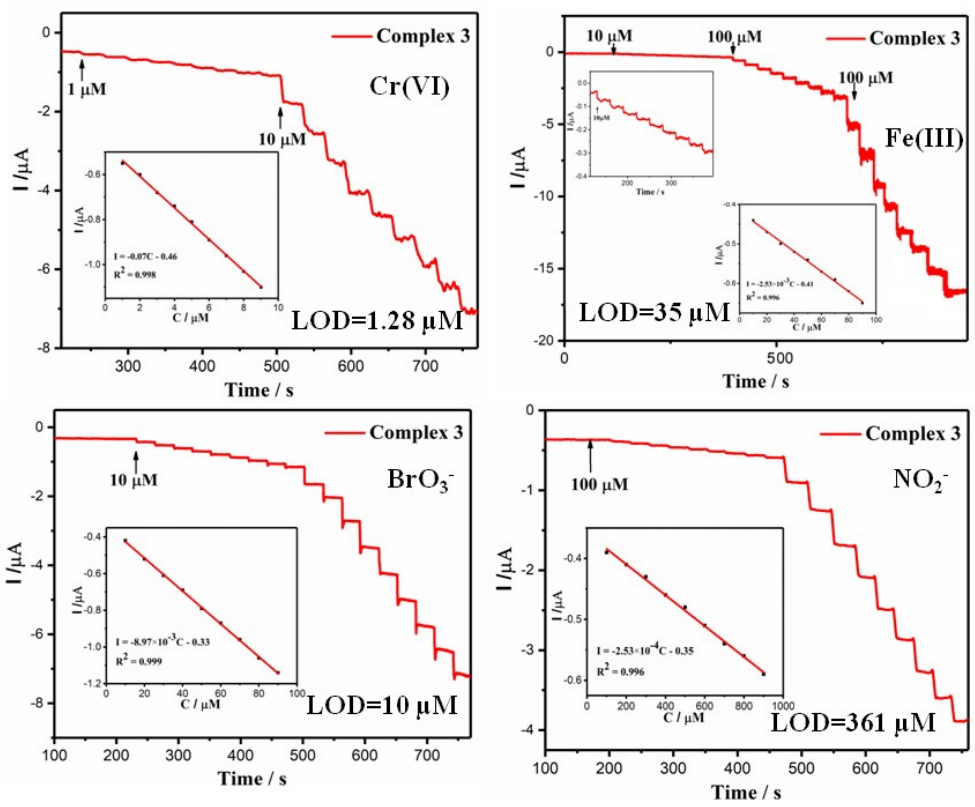

Fig. S9 Current response of **3**-CPE with successive addition of Cr(VI) (a) Fe(III) (b) BrO_3^- (c) and NO_2^- (d) into stirring 0.1 M H_2SO_4 + 0.5 M Na_2SO_4 electrolyte solution per 30 s interval (Inset: the plot of response current vs concentrations of substrate. Applied potential: -200 mV for **3**–CPE).

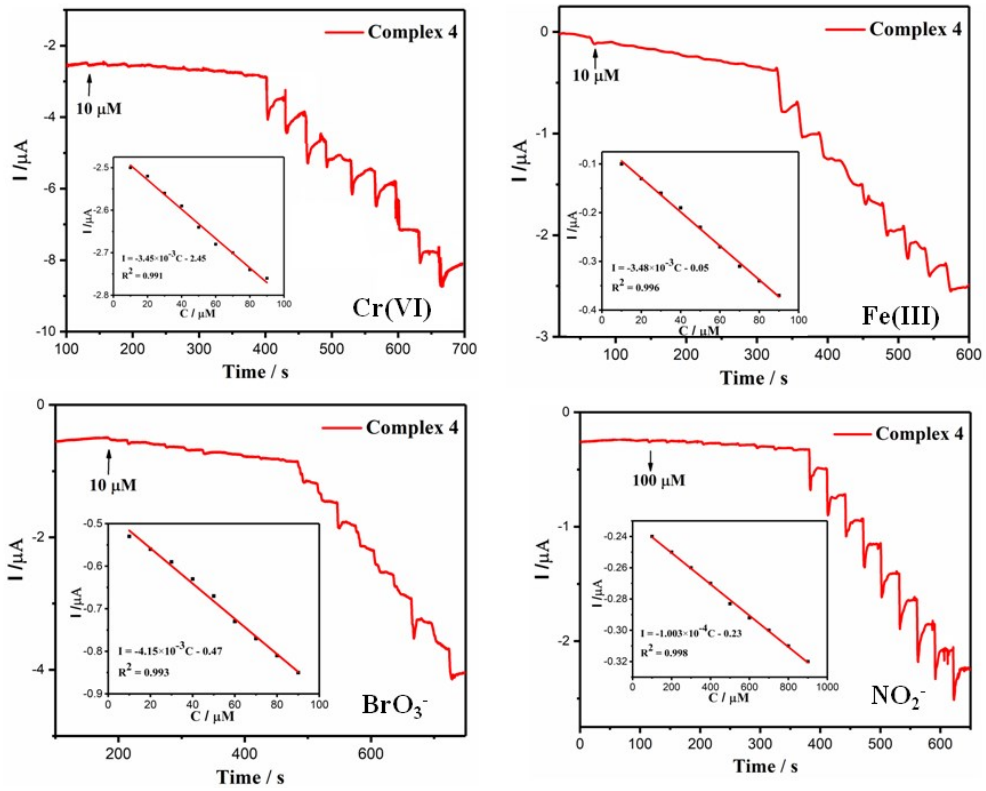

Fig. S10 Current response of **4**-CPE with successive addition of Cr(VI) (a) Fe(III) (b) BrO_3^- (c) and NO_2^- (d) into stirring 0.1 M H_2SO_4 + 0.5 M Na_2SO_4 electrolyte solution per 30 s interval (Inset: the plot of response current vs concentrations of substrate. Applied potential: -200 mV for **4**–CPE).

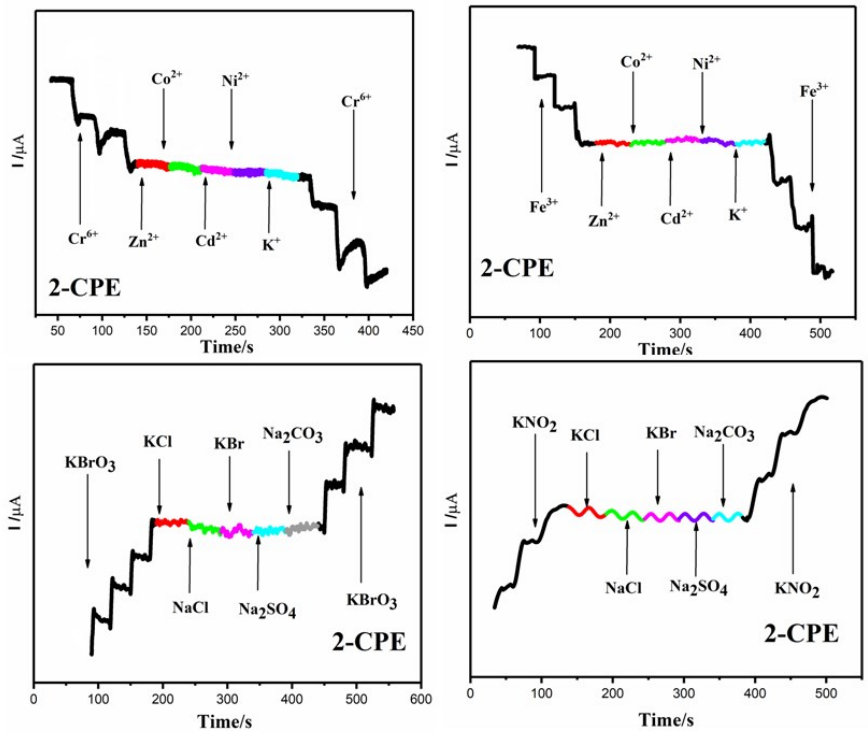

Fig. S11 Current response of **2**-CPE for Cr(VI) (a) Fe(III) (b) BrO_3^- (c) and NO_2^- (d) with addition of potential interference substances in 0.1 M H_2SO_4 + 0.5 M Na_2SO_4 electrolyte solution.

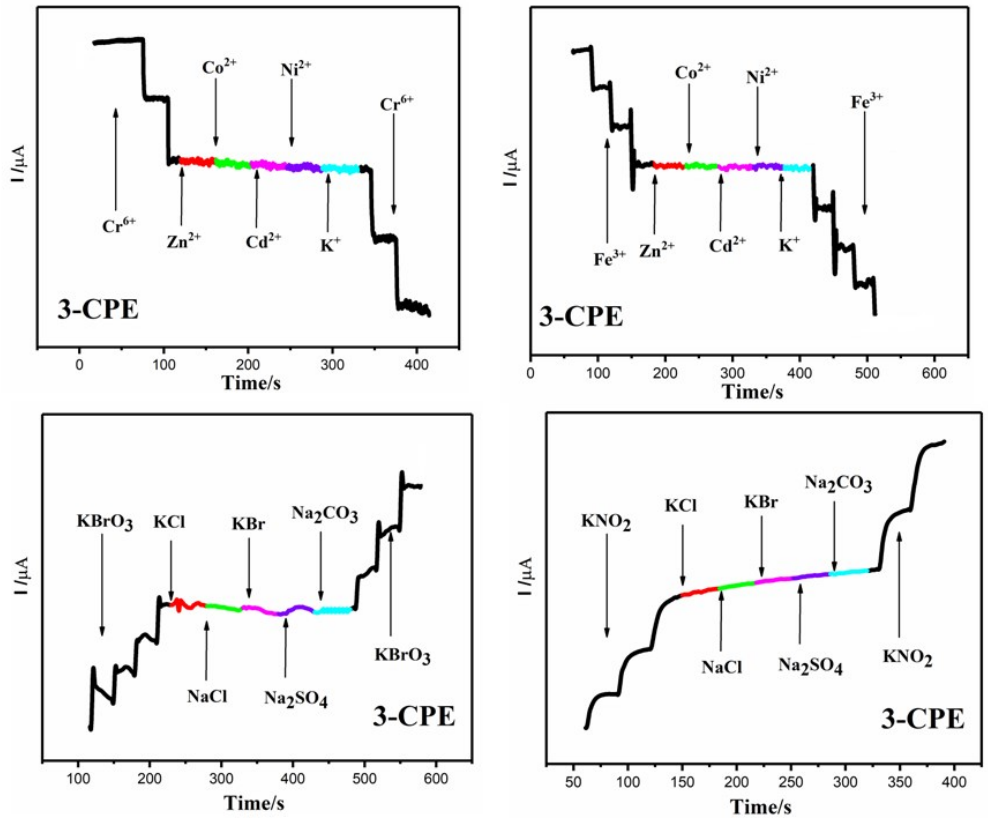

Fig. S12 Current response on **3**-CPE for Cr(VI) (a) Fe(III) (b) BrO_3^- (c) and NO_2^- (d) with addition of potential interference substances in 0.1 M H_2SO_4 + 0.5 M Na_2SO_4 electrolyte solution

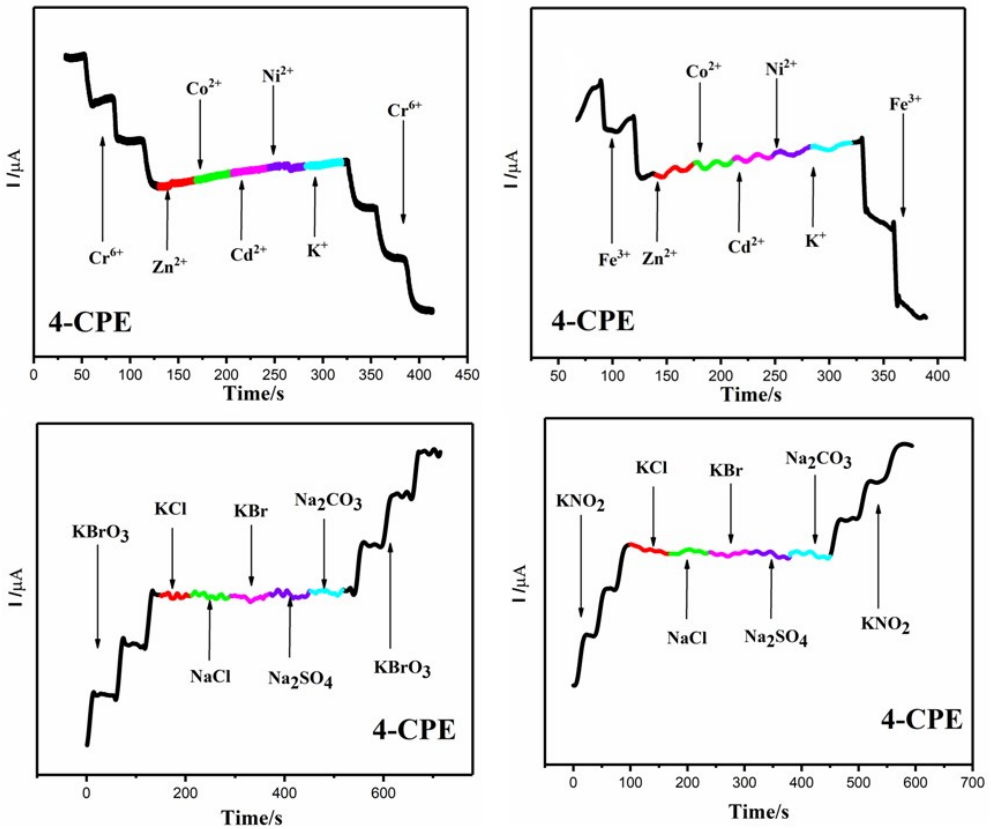

Fig. S13 Current response on **4**-CPE for Cr(VI) (a) Fe(III) (b) BrO_3^- (c) and NO_2^- (d) with addition of potential interference substances in 0.1 M H_2SO_4 + 0.5 M Na_2SO_4 electrolyte solution

Table. S4 Experimental data for detecting Cr(VI), Fe(III), BrO_3^- and NO_2^- using **1**~**4**-CPEs as amperometric sensors

Material		Cr(VI)	Fe(III)	BrO_3^-	NO_2^-
Detection limit (μmol L^{-1})	**1**-CPE	0.51	3.75	8.6	292
	2-CPE	30	48	22	166
	3-CPE	1.28	35	10	361
	4-CPE	33	32	27	1140
Linear Range (μmol L^{-1})	**1**-CPE	1-100	1-100	1-1000	100-10000
	2-CPE	10-1000	10-1000	10-1000	100-10000
	3-CPE	1-100	10-1000	10-1000	100-10000
	4-CPE	10-1000	10-1000	10-1000	100-10000
Sensitivity (μA cm^{-2} mM^{-1})	**1**-CPE	0.146	0.02	8.667×10^{-3}	2.566×10^{-4}
	2-CPE	4.95×10^{-3}	1.23×10^{-3}	6.7×10^{-3}	9.111×10^{-4}
	3-CPE	0.07	2.53×10^{-3}	8.97×10^{-3}	2.53×10^{-4}
	4-CPE	3.45×10^{-3}	3.48×10^{-3}	4.15×10^{-3}	1.003×10^{-4}

Table S5 Comparison of other work for detecting Cr(VI)

Electrode material	**Detection limit**	**Ref.**
$[HC_5H_6N_2]_6\{Co[Mo_6O_{12}(OH)_3(HPO_4)_3(H_2PO_4)]_2\}\cdot nH_2O$	0.026 μM	**38**
1-CPE	0.51μM	This work
AuSPE	4.4 μM	**39**
screen-printed carbon electrode	0.77 μM	**40**
AMC/MMT	5 μM	**41**
CCDs	1.17 μM	**42**

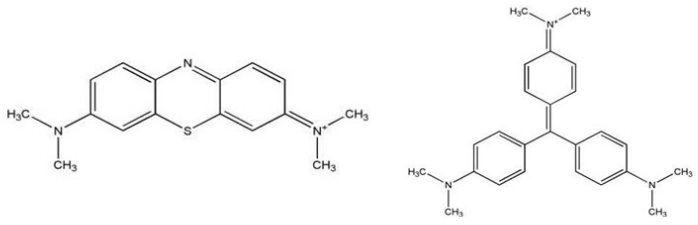

Scheme S1 Chemical structures of MB and GV.

Notes and references

S1. V. Dolomanov, L. J. Bourhis, R. J. Gildea, J. A. K. Howard and H. Puschmann, *J. Appl. Crystallogr.*, 2009, **42**, 339.